



This is a repository copy of *A dye-sensitised Schottky junction device fabricated from nanomaterials on a stainless steel substrate.*

White Rose Research Online URL for this paper:
<https://eprints.whiterose.ac.uk/117421/>

Version: Accepted Version

Article:

Ryall, N.E., Crook, R. and Weinstein, J.A. (2018) A dye-sensitised Schottky junction device fabricated from nanomaterials on a stainless steel substrate. *Materials Research Innovations*, 22 (4). pp. 231-236. ISSN 1432-8917

<https://doi.org/10.1080/14328917.2017.1302154>

Reuse

Items deposited in White Rose Research Online are protected by copyright, with all rights reserved unless indicated otherwise. They may be downloaded and/or printed for private study, or other acts as permitted by national copyright laws. The publisher or other rights holders may allow further reproduction and re-use of the full text version. This is indicated by the licence information on the White Rose Research Online record for the item.

Takedown

If you consider content in White Rose Research Online to be in breach of UK law, please notify us by emailing eprints@whiterose.ac.uk including the URL of the record and the reason for the withdrawal request.



eprints@whiterose.ac.uk
<https://eprints.whiterose.ac.uk/>



UNIVERSITY OF LEEDS

This is an author produced version of *A dye-sensitised Schottky junction device fabricated from nanomaterials on a stainless steel substrate*.

White Rose Research Online URL for this paper:
<http://eprints.whiterose.ac.uk/114144/>

Article:

Ryall, NE, Crook, R and Weinstein, JA (2017) A dye-sensitised Schottky junction device fabricated from nanomaterials on a stainless steel substrate. *Material Research Innovations*. ISSN 1432-8917

<https://doi.org/10.1080/14328917.2017.1302154>

This is an Accepted Manuscript of an article published by Taylor & Francis in *Material Research Innovations* on 17th March 2017, available online:
<http://www.tandfonline.com/10.1080/14328917.2017.1302154>



*promoting access to
White Rose research papers*

eprints@whiterose.ac.uk
<http://eprints.whiterose.ac.uk/>

A Dye-sensitised Schottky Junction Device fabricated from Nanomaterials on a Stainless Steel Substrate

N. Ryall^{a*}, R. Crook^a and J. Weinstein^b

^a School of Chemical and Process Engineering, University of Leeds, Leeds, UK

^b Department of Chemistry, University of Sheffield, Sheffield, UK

*Corresponding author: N. Ryall, School of Chemical and Process Engineering, Leeds, LS2 9JT
elner@leeds.ac.uk

A Dye-sensitised Schottky Junction Device fabricated from Nanomaterials on a Stainless Steel Substrate

Key words: Schottky barrier, steel, silver nanowires, TiO₂, sensitised

Dye-sensitised Schottky junction cells were fabricated on stainless steel using TiO₂ and silver nanowires. A titania sol was synthesised by a sol-gel process and was deposited on the substrate by dip coating, followed by sintering at 350°C for grade 304 stainless steel. Silver nanowires were drop cast from suspension and annealed. The current-voltage characteristics were measured and fit to the diode equation. The average I₀ value for a typical batch of anatase devices was 4.9×10^{-6} A cm⁻². The devices showed a UV response after treatment with tartaric acid and showed EQEs of 7.0 % in the UV at single wavelengths. It was possible to measure a small visible photocurrent for these devices following functionalisation with a ruthenium dye.

Introduction

Photovoltaic and photocatalytic cells with high efficiency, low cost, high stability and made from abundant materials provide a formidable fabrication challenge. There are a range of architectures of third generation solar cells which aim to reduce the need for the low defect single crystal films typically used in first generation silicon solar cells. [1] Whilst most commercial photovoltaic cells are manufactured from crystalline silicon, many promising second and third generation devices are emerging, with good efficiencies reported for thin film chalcogenides, perovskites, organic and dye-sensitised solar cells (DSSCs). [2] The sensitization of Schottky barriers to produce a photocurrent has also been demonstrated, though with low reported efficiencies. [3]

An example of a dye-sensitised Schottky barrier device was formed following the sensitization of a thin gold film on TiO₂ with merbromin dye. [3] The proposed mechanism for the transport of electrons from the dye was by ballistic transport through the gold film. [3]

A similar architecture can also be used to produce Schottky barrier cells from p-type materials namely PbSe nanocrystals, which showed an impressive efficiency of 2.1 % under AM 1.5G, but with limited stability in air. [4] Further, a Schottky barrier device was formed between a TiO₂ film functionalised with an inorganic dye and a thermally evaporated gold contact. [5] The dye functionalisation resulted in altered diode characteristics, with rectification increased by several orders of magnitude and showing a limited photoresponse, all achieved with the Ru(dcbpy)₂(NCS)₂ (where dcbpy is (2,2'-bipyridine)-4,4'-dicarboxylic acid) dye. [5]

As has been widely studied on a variety of substrates, Schottky barrier height is impacted by surface states and DFT studies of TiO₂ appear to corroborate this for TiO₂/noble metal systems. Schottky barrier height has been studied using a DFT model of a TiO₂ and Au interface and this suggests the Schottky barrier can decrease from 0.87 eV to 0.15 eV when there are oxygen defects present on the TiO₂ surface. [6]

A Schottky barrier can be formed between nanoparticulate silver and gold on the semiconductor in DSSCs to improve the charge collection at the semiconductor/solvent interface. The Schottky barrier increases the residency time of electrons in the semiconductor, as observed by measuring the dynamics of recombination of a fluorescent dye on ZnO nanorods modified by Au nanoparticles. [7] There is also evidence to suggest a Schottky barrier formed between compact TiO₂ and an Indium Tin Oxide (ITO) substrate in a DSSC can cause current loss, by reducing the current collection rate at the back electrode of a DSSC. [6]

This work focussed on the fabrication of Schottky junctions that can be made under standard laboratory conditions utilising dip coating and drop casting. The devices can be fabricated on stainless steel with a titania sol, with a top contact of silver nanowires from a suspension. These devices can then be functionalised with dyes and a small visible photocurrent can be measured. Electrons from the excited dye molecule can transfer from the dye excited states to the TiO₂ conduction bands for collection at the substrate. Electrons are proposed to transfer from the silver nanowires to the dye, as illustrated in Figure 1 to repopulate the dye ground state. Under illumination of the device under UV light, the device will function as a conventional Schottky junction cell (Figure 1)

[Figure 1]

Figure 1: Illustration of the mode of action of a dye-sensitized Schottky barrier device formed between silver nanowires and a semiconductor (not to scale).

In the examples of such devices found in the literature, noble metals have been thermally evaporated onto substrates under vacuum, or deposited electrochemically. [3][5] However, due to the use of dispersed silver nanowires, several different areas used in this work must be defined and are illustrated in Figure 2. The geometric area is defined as the physical area of the device being equal to the area of the steel substrate. The shadow area is defined as the coverage of the silver nanowires, as measured from a typical SEM image. The junction area is defined as the area available for functionalisation is that around the nanowires and depends on the lateral extent of the Schottky barrier.

[Figure 2]

Figure 2: Demonstrating the different defined areas of the device.

Experimental procedure

In a typical TiO₂ sol synthesis, 12 ml of isopropyl alcohol, 1 ml of deionised water and 1 ml nitric acid (70 %) are stirred vigorously. 0.5 ml of titanium isopropoxide (97 %) was added dropwise and stirred for > 30 mins yielding a pale yellow transparent viscous liquid. For an anatase sol, this liquid is hydrolysed for 8 hours under reflux. Following this, ammonia solution (30%) was added dropwise with stirring until it is above pH 7 yielding a viscous sol. The steel is cut into small (~1cm²) pieces and rinsed with isopropyl alcohol. Dip coating was

performed by hand, with excess sol removed by capillary action on lab tissue. Typically 2-4 coats were applied and each coat was left to dry at room temperature before the next dip coating. In a typical device the TiO₂ films were then sintered at 350°C for 90 minutes in a furnace. When cool, the devices are drop cast with 5 µL aliquots using a micropipette, totalling 10-25 µL of a 0.25% m/v silver nanowire (AgNWs) suspension in isopropanol (stated nanowire dimensions 60 nm × 10 µm, diluted from 0.5% m/v suspension). The silver nanowires were annealed at 235°C for 20 minutes to reduce junction resistance. To study the functionalisation of the devices with dye, the devices were soaked in a ruthenium dye (Ru(dcbpy)₂Cl₂) in ethanol solution provided by J. Weinstein. The current-voltage measurements have been performed using a Gamry Potentiostat between -1 V and 1V, using a 100 Ω resistor in series with the device to limit the current travelling through the device. Photocurrents have been measured using an arc lamp monochromator (Bentham SSM150Xe Programmable light source) controlled with a program written in-house in C by R.Crook and calibrated with a commercial UV enhanced Si photodiode (Si Series 7 OSD5.8-7 Q Centronic Photodiode).Mathematical analysis of the IV measurements was performed with MatLab software. All chemicals were purchased from Sigma Aldrich and used without further purification unless otherwise stated. 304 and 316 stainless steel was purchased from RS components and Fischer Scientific. ITO coated glass was purchased from Sigma Aldrich.

Results and Discussion

Fabrication

Diodes were fabricated on stainless steel by dip coating the substrate in a TiO₂ sol and then depositing and annealing silver nanowires. Two grades of steel were used; 304 and 316 stainless steel (304 SS and 316 SS respectively). These grades differ in their composition and are compared in Table 1.

Steel grade	Proportion of element / %				
	Cr	Ni	Mn	Mo	Si
304	17.5-19.0	8.0-11.0	2.00	-	1.00
316	16.0-18.0	10.0-14.0	2.00	2.0-3.0	0.75

Table 1: Comparison of two grades of steel

Steel forms chromia plates when it is heated, this is one of the ways in which steel self-protects against corrosion and these layers depend on the grade of steel used and its preparation method [8]. The chromia films which have slower growth kinetics than iron oxides act as a barrier to the diffusion of cations from the steel. [9]

The temperature at which diodes could be made depended on the grade of steel used. Whilst devices on 304 SS could be formed at 350 °C but not above these temperatures, the same attempts made on 316 SS were unsuccessful. Only devices formed at higher temperatures, or following a pre-treatment stage of heating the steel to high temperature prior to sintering of the TiO₂ films gave diode IV characteristics on 316 SS. Given that the protective films which form on steel prevent the diffusion of cations, the temperature dependence for the formation of Schottky barriers could be due to diffusion of metal ions through the TiO₂ film.

When 316 SS was heat treated and the oxide manually removed prior to sintering of the TiO₂ film, the devices formed were ohmic, compared to rectifying when the layer was left intact. The diffusion of ions could cause a short circuiting of the Schottky barrier, by formation of ohmic contacts at the interface with the silver nanowires.

Metal diffusion through titania from the substrate has been reported in the literature, for instance, a 90 nm TiO₂ film on 304 SS had 7 mol % Fe content following annealing at 400 °C for 1 hour, and this was detected at the surface of the film in the form of rhombohedral Fe₂O₃. [10] Similarly, the impact of metal diffusion through TiO₂ films for DSSCs has also been studied. Sn diffusion through TiO₂ films used in DSSC's has been measured to occur at a rate of $3.2 \times 10^{-5} \mu\text{m}^2$ in a doctor bladed TiO₂ film at 450 °C. [11]

EDX measurements (Figure 3) of devices made on 304 SS show high levels of Fe and Cr in regions both where the film is thin (Figure 3).

[Figure 3]

Figure 3: Top row, left: SEM image of 316 heated steel showing chromia plates. Top row, right: SEM image of thin TiO₂ coating on 304 type steel. Middle and bottom: EDX images of top right SEM image; (centre left) O K α 1, (centre right) Ti K α 1, (bottom left) Cr K α 1 and (bottom right) Fe K α 1.

Current-Voltage Characteristics

Device IV curves were measured with a potentiostat and modelled using a modified ideal diode equation and thermionic emission theory, described by the following equations.

$$I = I_0 \left(\left(\exp \frac{qV}{nkT} \right) - 1 \right) + \frac{V}{R_s} \quad (1)$$

Where I = device current

q = elementary charge

n = diode ideality factor

V = device voltage
 R_s = shunt resistance
 k = Boltzmann constant
 T = absolute temperature
 I_0 = reverse saturation current

$$I_0 = SA^*T^2 \left(\exp \frac{-\phi_s}{kT} \right) \quad (2)$$

Where S = junction area
 A^* = modified Richardson constant
 Φ_s = Schottky barrier height

The shunt resistance incorporates electron transport through the device by other mechanisms.

Typical measurements of current and voltage (IV measurements) between room temperature and 100 °C can be seen in Figure 4 for a device of $\sim 1 \text{ cm}^2$.

[Figure 4]

Figure 4: IV curves at a range of temperatures for a typical diode.

To estimate the series resistance, differential resistance was measured between 0.95 and 1.0 V. The outcome of fitting was generally good, 1406 measurements of 487 devices gave R^2 values above 0.99. A set of control devices, made from anatase (24 devices) and amorphous (10 devices) sols of TiO_2 and are shown in Table 2. Results for ohmic devices or those with lower R^2 values were discarded.

Control devices	Average I_0 / A	R_{shunt} / Ω	R_{series} / Ω
Amorphous	3.7×10^{-5}	7.2×10^3	1260
Anatase	4.9×10^{-6}	4.2×10^5	190

Table 2: Showing I_0 values for a single series of control devices

Diode properties and temperature

The IV curves of some devices were measured at a range of temperatures. It was found that the I_0 values increased exponentially with temperature up to 100 °C, followed by a linear

decrease. This is possibly due to competition from other competing mechanisms at higher temperatures, in particular, there is likely to be an interface between the TiO₂ layer and a p-type chromia layer on the steel or due to a changing TiO₂ interface with silver. For this reason, in the thermal analysis, only results below 100°C were used. The error inherent in this method include the problem of temperature fluctuations during the measurements, for which reason, many of the analyses showed poor correlation of I₀ with temperature. Fitting using Equation 2 gave Richardson plots (Figure 5), allowing the estimation of Schottky barrier height (Table 3).

[Figure 5]

Figure 5: Example Richardson plot of reverse saturation current against temperature.

	SBH (thermionic emission theory) / eV	R ²
1	0.91	0.98
2	0.56	0.91
3	1.27	0.94

Table 3: Values from Richardson plots for a range of devices.

The calculated Schottky barrier heights from a range of devices correlated well with the R² of the fit of the Richardson plot (R² > 0.8). The best estimation of the barrier height, at 0 K, is ~0.91 eV, due to its high R² value.

Junction area estimates

Although the Richardson plots could be used to deduce the active area of the device, the logarithmic nature of the plots compounded error and resulted in drastically different estimated areas from devices of similar area. The vacuum level of the Richardson constant is 120 A cm⁻² K⁻² but this is corrected for the effective masses of electrons in a material being different to that in a vacuum. [12] The best fit, that of Figure 5, gives an area of 0.087 cm², using a reported Richardson constant of 24 A cm⁻² K⁻² for TiO₂. [12]

A typical device had 59 µg of silver nanowires deposited and assuming they have a density similar to that of bulk silver and their dimensions are as stated by the supplier, on average 10 µm in length and 60 nm diameter, this gives an estimated 3 × 10⁹ wires per device. This is consistent with counting the silver nanowires over a small area of 6.25 µm² by SEM and extrapolation to the full area of the device (Figure 6).

This equals an effective surface area of the silver nanowires of ~3.6 cm² per device, using their stated dimensions. Comparing to the Richardson plot estimate of 0.087 cm², this equates to 2.4% of the wire area. This suggests a low proportion of the silver nanowires are in contact with TiO₂ and are contributing to the junction area of the Schottky barrier. However, some of these will be necessary to forming a conductive mesh on the device, so bringing disparate junction areas into contact and to reduce series resistance.

[Figure 6]

Figure 6: SEM images of a typical silver nanowire device, a $6.25 \mu\text{m}^2$ section was analysed to estimate the area covered by silver nanowires by extrapolation.

A report of a 17 mA/cm^2 current flowing through a low resistivity $12 \Omega/\text{sq}$. silver nanomesh has been shown to fail due to heating, with a calculated current density of $4 \times 10^4 \text{ A/cm}^2$ occurring in the nanowires, providing an estimate for failure of the nanowires due to current density. [13] This is higher than the densities calculated for even the smallest junction area estimates in this work.

Photocurrent

Photocurrents under UV light were seen for rectifying devices, however they were very small. Surface states can provide recombination sites, and additives to passivate surface states have been used to give higher efficiencies in DSSCs. [14] For this reason, a range of adsorbents were used in an attempt to improve the UV response of these devices. It was found that tartaric acid was a particularly effective additive.

It was also found that the films typical for the amorphous devices showed little evidence of crystallinity apart from peaks attributable to austenite iron oxides that are the same in the heat treated steel substrate. Typical literature methods for the production of anatase TiO_2 sols rely on a prolonged heating step, at an elevated temperature. For this reason, a method was used to produce a more crystalline sol. New sols underwent an 8 hour reflux step, resulting in films that showed very broad peaks that correspond to the anatase phase. The peaks are significantly broader than commercial TiO_2 P25 nanopowder, suggesting small crystallite size or defects. This is likely in these samples due to the diffusion of metals from the substrate and imperfect crystallisation. The partially anatase films show a considerable photoresponse in the UV region compared to the amorphous devices (Figures 7 and 8).

Literature DFT studies on amorphous TiO_2 have found that the energy for formation of the oxygen vacancy in TiO_2 is much lower than in crystalline forms, resulting in relatively good hole transport and that the trapping of holes also occurs more easily. [15] Hole trapping may be a significant loss mechanism in the amorphous devices given the n-type nature of conduction in TiO_2 .

Both amorphous and anatase devices, with tartaric acid showed higher photocurrents when illuminated with UV light, as shown in Figures 7 and 8.

[Figure 7]

Figure 7: UV responses for an amorphous TiO_2 device.

[Figure 8]

Figure 8: UV responses for an anatase TiO_2 device.

Current densities of several hundred nA cm^{-2} and up to $1.3 \mu\text{A cm}^{-2}$ was seen in the UV region, corresponding to 7.0 % EQE at a single wavelength. A series of passivated devices, showing a range of UV responses are shown in Figure 9.

[Figure 9]

Figure 9: UV response for a range of devices, showing a photocurrent density of several hundred nA cm^{-2} .

Modification

Ruthenium dyes containing acid bipyridines show excellent absorption coefficients, allow binding to TiO_2 and were used in the first DSSCs. [16] Previous similar work on functionalisation of a TiO_2 Schottky barrier device found it was possible to measure a photocurrent following the functionalisation of a TiO_2 Schottky barrier with a ruthenium dye. [5]

As such, devices were soaked in $\text{Ru}(\text{dcbpy})_2\text{Cl}_2$, where dcbpy is 2,2'-bipyridine-4,4'-dicarboxylic acid, to sensitize the devices. $\text{Ru}(\text{dcbpy})_2\text{Cl}_2$ sensitised devices gave lower I_0 values and higher maximum currents on average than the control devices. Some preliminary work shows that this phenomenon is not unique to $\text{Ru}(\text{dcbpy})_2\text{Cl}_2$, with $\text{Co}(\text{bpy})_3^{2+} \text{NO}_3^{2-}$ (where bpy is 2,2' bipyridine) and organic acids showing improvements to the IV characteristics of the device, suggesting this is not limited to asymmetric ruthenium dyes.

It is possible to achieve a visible photocurrent using a device functionalised with $\text{Ru}(\text{dcbpy})_2\text{Cl}_2$ dye, as shown in Figure 10. The unfunctionalised device shows no photocurrent in the visible region.

These visible responses were uncommon on the amorphous and unpassivated films. Anatase devices functionalised with $\text{Ru}(\text{dcbpy})_2\text{Cl}_2$ and passivated with tartaric acid, and showed a limited photocurrent, dwarfed by the UV response.

[Figure 10]

Figure 10: Photocurrent response from a **range** of devices functionalised with $\text{Ru}(\text{dcbpy})_2\text{Cl}_2$ showing some limited **and varied** photocurrent in the visible region.

The measured photocurrents are extremely small, for reference a commercial silicon photodiode provides a maximum of $31.3 \mu\text{A /cm}^2$ at $\sim 500 \text{ nm}$ under similar conditions. **There is also marked variation between the devices which is likely to be due to the variation in active areas for the devices.**

For the best device, a peak external quantum efficiency of $6.7 \times 10^{-3} \%$ is found at 520 nm. However, this demonstrates that this architecture functions and that charge separation has occurred at the interface.

Of the whole area of the device, only the junction area is likely to be optically active and therefore the efficiencies will be higher considering just this area, compared to the geometric area of the device of 1 cm^2 . Table 4 shows adjusted efficiencies. The shadow area is taken to be 0.13 cm^2 and is an estimate for the coverage of the silver nanowires. The best estimate from the thermionic emission analysis, 0.087 cm^2 , is used for junction area. The generated current under visible and UV light are due to differing mechanisms, but in both cases, the extent of the area of the junction is going to be important to the measurement of EQE.

It is likely that the overall efficiencies of the devices can be further improved by optimisation of the geometry of the device. For instance, by functionalising the whole area of the nanowires, an area 3 times larger than that of the geometric area would increase the available junction area and the photocurrents could be improved drastically.

Device type	λ / nm	EQE (by GE) / %	EQE (by SA) / %	EQE (by JA) / %
Amorphous	300	0.016	0.12	1.8
Anatase	300	7.0	53.8	80.5
Ru(dcbpy) ₂ Cl ₂ sensitised device	520	0.0067	0.052	0.8

Table 4: External Quantum efficiency (EQE) has been calculated as a proportion of the geometric area (GE), taken to be 1 cm^2 and shadow area, taken to be 0.13 cm^2 and the best estimate of junction area, taken to be 0.087 cm^2 .

Further improvements could be made by better passivation and fabrication strategies, particularly in the control of crystallisation of TiO_2 . Also, dyes can be altered continuously and optimised loadings of dyes, co-adsorbents and an improved architecture could all improve efficiency.

Conclusion

A Schottky barrier can be formed over a large area between silver nanowires and TiO_2 , on a stainless steel substrate. A range of methods have been used but the best results are obtained for 304 stainless steel dip coated in a titania sol which had undergone a reflux step for 8 hours, followed by sintering at $350 \text{ }^\circ\text{C}$ for 90 minutes followed by drop cast silver nanowires. There is no doubt that this process could be improved by further improvements to the sol and to the substrate, particularly to improve the crystallinity of the films used. This is a cheap process requiring no specialist equipment, which may allow the large scale synthesis and

improvement of these systems and their application. The reverse saturation currents could doubtless be improved by small molecule mediation and diode characteristics are altered by acids. Some cells functionalised with a ruthenium dye show a small photocurrent response to visible light, which whilst not at the moment being large enough to be of any practical value, demonstrates the potential use of these cells, as well as showing potential to give information about how a dye and TiO₂ interact in these systems. The sensitivity of these devices to temperature, pH and UV light could also lead to their use as sensors.

Geotag:

University of Leeds, LS2 9JT

53°48'34.7"N 1°33'25.8"W

Acknowledgment

This work was supported by the EPSRC and the CDT in Molecular-Scale Engineering.

References

- (1) M.A. Green, *Physica E*, 14 (2002), 65-70
- (2) M.A. Green et al., *Prog. Photovolt: Res. Appl.*, 24, (2016), 905-913
- (3) E.W. McFarland and J. Tang, *Nature* 421 (2003) 616
- (4) J. Luther et al., *Nano letters* 8 (2008) 3488
- (5) Th. Dittrich et al., *Thin Solid films* 516 (2008) 7234
- (6) Marri and Ossicini, *Solid State Communications* 147 (2008) 205
- (7) T. Bora et al., *Belstein J. Nanotechnology* 2 (2011) 681
- (8) K.A. Habib et al., *Int. J. Corrosion* (2011) Article ID 824676, 10 pages
- (9) A.C.S. Sabioni et al., *Materials Science and Engineering A*, 392, 2005, 254-261
- (10) Y. Zhu, et al., *J. Mat. Chem.* 11 (2001) 1864
- (11) J. Kabre and R.J. LeSuer, *J. Phys.Chem. C*. 116 (2012) 18327
- (12) J. Y. Park et al., *Nano Letters* 8 (2008) 2388
- (13) H.H. Khaligh and I.A. Goldthorpe, *Nano. Res. Lett.* 8 (2013) 235
- (14) Y. Lee et al., *J. Phys. Chem. C* 116 (2012) 6770
- (15) H.H. Pham and L. Wang, *Phys. Chem. Chem. Phys.* 17 (2015) 541-550
- (16) M. Gratzel and B. O'Regan, *Nature* 353 (1991) 737

Words: 3526

A Dye sensitised Schottky Junction Device fabricated from Nanomaterials on a Stainless Steel Substrate (Figures)

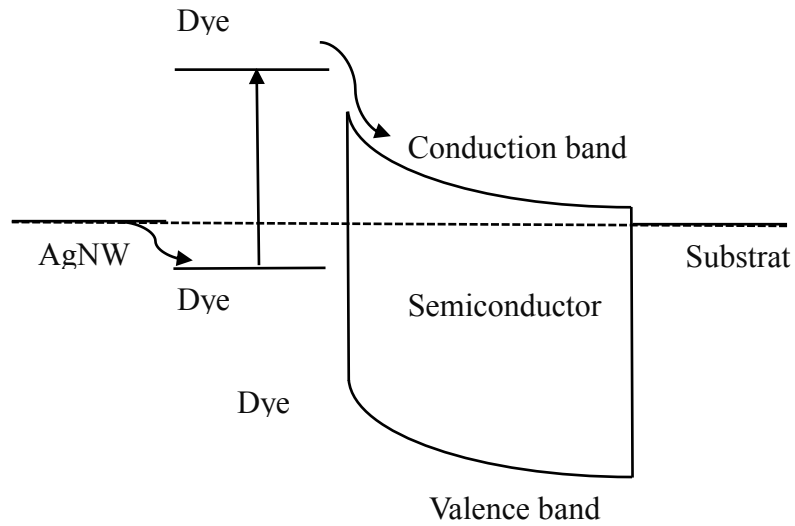
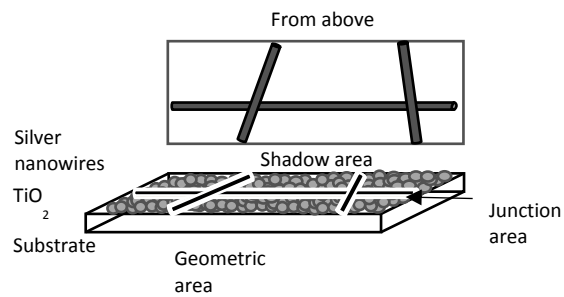


Figure 1: Illustration of the mode of action of a dye sensitized Schottky barrier device formed between silver nanowires and a semiconductor (not to scale).



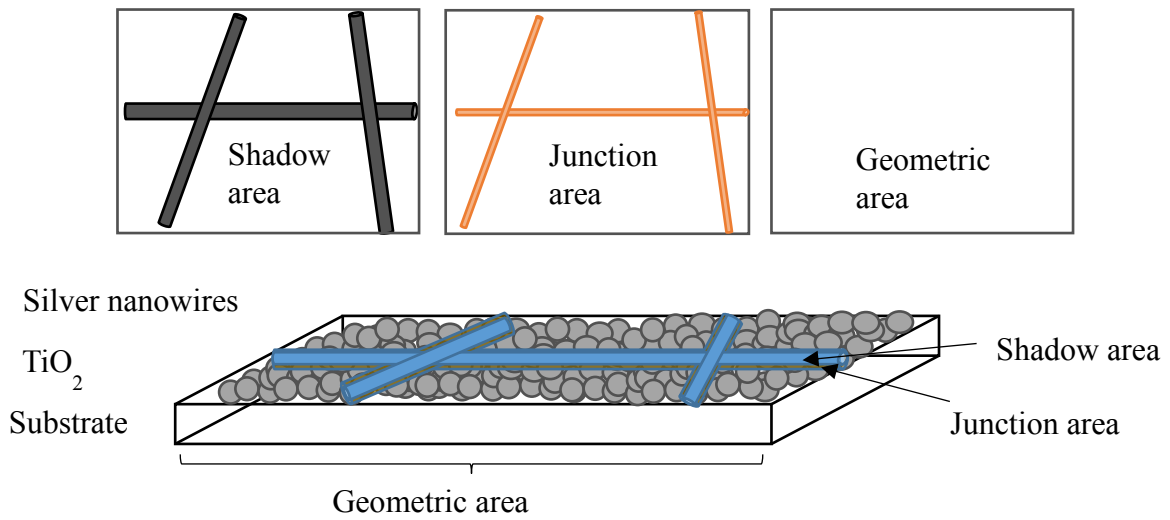
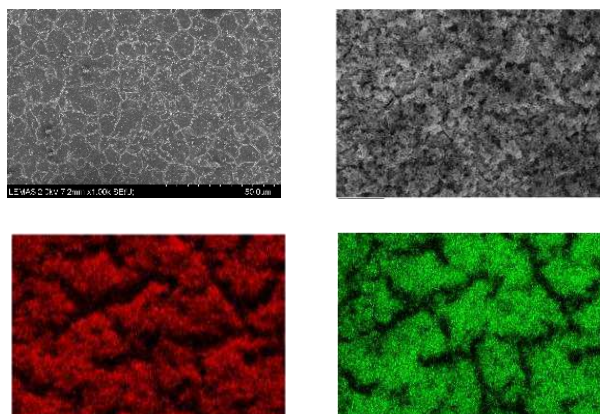


Figure 2: Demonstrating the different defined areas of the device.

Steel grade	Proportion of element / %				
	Cr	Ni	Mn	Mo	Si
304	17.5-19.0	8.0-11.0	2.00	-	1.00
316	16.0-18.0	10.0-14.0	2.00	2.0-3.0	0.75

Table 1: Comparison of two grades of steel



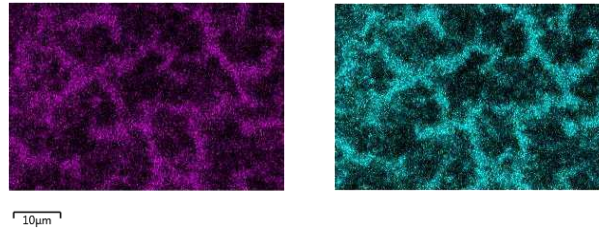


Figure 3: Top row, left: SEM image of 316 heated steel showing chromia plates. Top row, right: SEM image of thin TiO_2 coating on 304 type steel. Middle and bottom: EDX images of *top right SEM image*; (*centre left*) *O Ka1*, (*centre right*) *Ti Ka1*, (*bottom left*) *Cr Ka1* and (*bottom right*) *Fe Ka1*.

$$\text{Equation 1: } I = I_0 \left(\left(\exp \frac{qV}{nkT} \right) - 1 \right) + \frac{V}{R_s}$$

Where I = device current

q = elementary charge

n = diode ideality factor

V = device voltage

R_s = shunt resistance

k = Boltzmann constant

T = absolute temperature

I_0 = reverse saturation current

$$\text{Equation 2: } I_0 = SA^*T^2 \left(\exp \frac{-\Phi_s}{kT} \right)$$

Where S = junction area

A^* = modified Richardson constant

Φ_s = Schottky barrier height

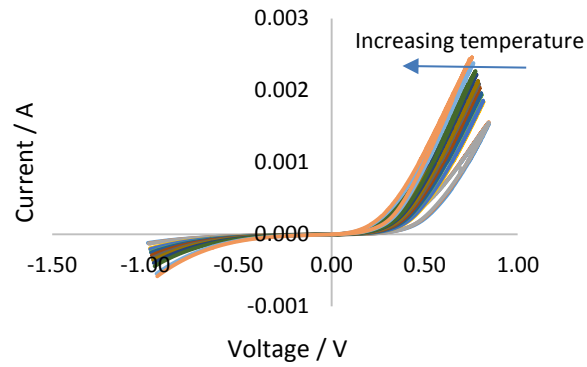


Figure 4: IV curves at a range of temperatures for a diodic device.

Control devices	Average I_0 / A	R_{shunt} / Ω	R_{series} / Ω
Amorphous	3.7×10^{-5}	7.2×10^3	1260
Anatase	4.9×10^{-6}	4.2×10^5	190

Table 2: Showing I_0 values for a single series of control devices

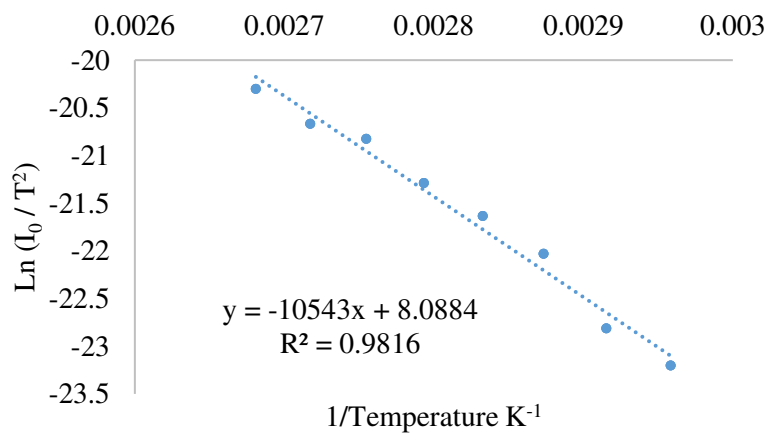


Figure 5: Example Richardson plot of reverse saturation current against temperature.

	SBH (thermionic emission theory) / eV	R ²
1	0.91	0.98
2	0.56	0.91
3	1.27	0.94

Table 3: Values from Richardson plots for a range of devices.

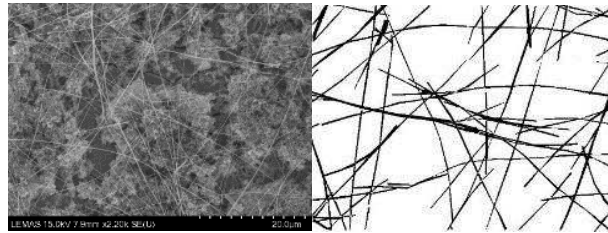


Figure 6: SEM images of a typical silver nanowire device, a section was analysed to find the area covered by silver nanowires.

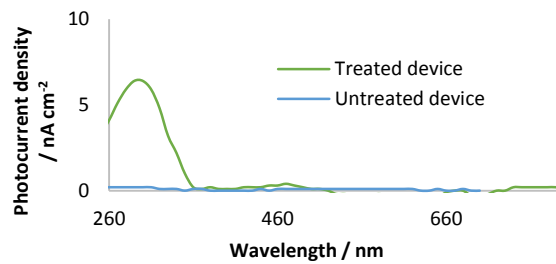


Figure 7: UV responses for an amorphous TiO₂ device.

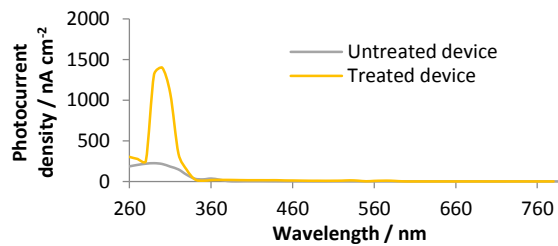


Figure 8: UV responses for an anatase TiO₂ device.

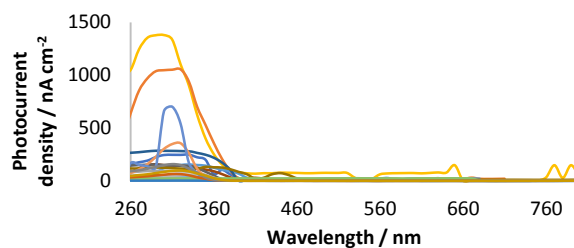


Figure 9: UV response for a range of devices, showing a photocurrent density of several hundred nA cm^{-2} .

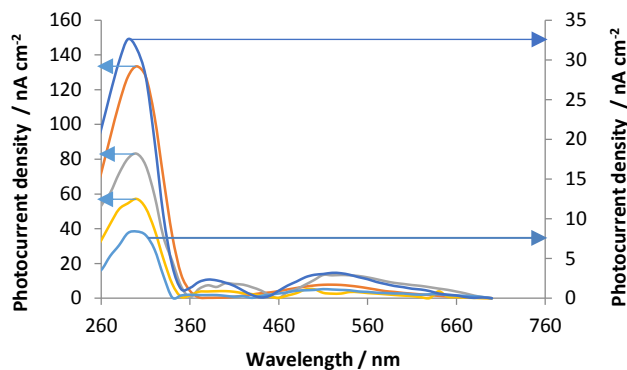


Figure 10: Photocurrent response from a series of devices functionalised with $\text{Ru}(\text{dcbpy})_2\text{Cl}_2$ showing some limited photocurrent in the visible region.

Device type	λ / nm	EQE (by GE) / %	EQE (by SA) / %
Amorphous	300	0.016	0.12
Anatase	300	7.0	53.8
$\text{Ru}(\text{dcbpy})_2\text{Cl}_2$ sensitized device	520	0.0067	0.052

Table 4: Efficiency has been calculated as a proportion of the geometric area, shadow area and junction area.